

Growth of $(\text{WO}_3)_n$ Rectangular Structures through a LMO–Organic Precursor Route

Shuping Pang, Fangfang Jian,* and Lei Wang

The Laboratory of New Materials and Functional Compounds, Qingdao University of Science and Technology, Qingdao 266042, P. R. China

Received July 25, 2007

A LMO–organic (LMO = layered metal oxide) hybrid precursor route has been developed to synthesize rectangular $(\text{WO}_3)_n$ structures. In the present work, regular rectangular orthorhombic $(\text{WO}_3)_n$ has been fabricated by a thermal decomposition of the as-synthesized rectangular $[\text{WO}_3(\text{bpy})_{0.5}]_n$ (bpy = 4,4'-bipyridine) precursor, which is formed by a process of intercalation, coordination, and self-assembly using the hydrothermal treatment of $(\text{WO}_3)_n$ and 4,4'-bipyridine. The precursor and final products were characterized by field-emission scanning electron microscopy, transmission electron microscopy, electron-induced X-ray fluorescence analysis, X-ray diffraction analysis, derivative thermogravimetry analysis, and thermogravimetric analysis.

Introduction

Controlling the shape of the materials is one of the most challenging issues presently faced by synthetic inorganic chemists.^{1,2} It is well-known that the physical, optical, and electronic properties of materials are dependent on their shape when their sizes are reduced to micrometer- and nanometer-scale dimensions.³ Surfactant-assisted synthesis methods take an important role in materials science. Reverse micelle and microemulsion techniques have been used to fabricate materials with specific size and morphology because of their soft template effect and selective absorbing property on different planes of seeds.^{4,5} Nowadays, a new kind of inorganic–organic precursor method has attracted more and more attention for its advantages in controlling phase and morphologies.^{6–8} LMO–organic (LMO = layered metal oxide) hybrid materials are an important category of inorganic–organic hybrid materials with their interesting interlayer structures.^{9–11} $(\text{WO}_3)_n$ represents an important wide

band gap semiconductor. It has been used in many areas including flat panel displays, photoelectrochromic “smart” windows, optical modulation devices, writing–reading–erasing optical devices, gas sensors, humidity and temperature sensors, and so forth.^{12–17} Although so many $(\text{WO}_3)_n$ structures including $(\text{WO}_3)_n$ nanowires,^{18,19} films,^{20,1} hollow spheres,²² and networks²³ have been widely synthesized, the preparation of rectangular $(\text{WO}_3)_n$ is still a primary challenge for scientists. Herein, we report the LMO–organic hybrid precursor route to synthesize rectangular $(\text{WO}_3)_n$ by the

* To whom correspondence should be addressed. E-mail: ffj2003@163169.net.

- (1) Sun, Y.; Xia, Y. *Science* **2002**, *298*, 2176.
- (2) Lee, K.; Seo, W. S.; Park, J. T. *J. Am. Chem. Soc.* **2003**, *125*, 3408.
- (3) Polleux, J.; Gurlo, A.; Barsan, N.; Weimar, U.; Antonietti, M.; Niederberger, M. *Angew. Chem., Int. Ed.* **2006**, *45*, 261.
- (4) Patel, A. A.; Wu, F.; Zhang, J. Z.; Torres-Martinez, C. L.; Mehra, R. K.; Yang, Y.; Risbud, S. H. *J. Phys. Chem. B* **2000**, *104*, 11598.
- (5) Wolcott, A.; Kuykendall, T. R.; Chen, W.; Chen, S.; Zhang, J. Z. *J. Phys. Chem. B* **2006**, *110*, 25288.
- (6) Xiong, Y.; Xie, Y.; Li, Z.; Wu, C. *Chem.–Eur. J.* **2003**, *9*, 1645.
- (7) Soulantica, K.; Maisonnat, A.; Fromen, M. C.; Casanove, M. J.; Lecante, P.; Chaudret, B. *Angew. Chem., Int. Ed.* **2001**, *40*, 448.
- (8) Yang, X.; Shao, C.; Guan, H.; Li, Gong, X. *J. Inorg. Chem. Commun.* **2004**, *7*, 176.

- (9) Yan, B.; Xu, Y.; Goh, N. K.; Chia, L. S. *Chem. Commun.* **2000**, 2169.
- (10) Wei, X. M.; Zeng, H. C. *Chem. Mater.* **2003**, *15*, 433.
- (11) Chen, Z.; Yang, Y.; Qiu, J.; Yao, J. *Langmuir* **2000**, *16*, 722.
- (12) Koltypin, Y.; Nikitenko, S. I.; Gedanken, A. *J. Mater. Chem.* **2002**, *12*, 1107.
- (13) Kim, Y. S.; Ha, S. C.; Kim, K.; Yang, H.; Choi, S. Y.; Kim, Y. T.; Park, J. T.; Lee, C. H.; Choi, J.; Paek, J.; Lee, K. *Appl. Phys. Lett.* **2005**, *86*, 213105.
- (14) He, Y.; Wu, Z.; Fu, L.; Li, C.; Miao, Y.; Cao, L.; Fan, H.; Zou, B. *Chem. Mater.* **2003**, *15*, 4039.
- (15) Chatten, R.; Chadwick, A. V.; Rougier, A.; Lindan, P. J. D. *J. Phys. Chem. B* **2005**, *109*, 3146.
- (16) Labidi, A.; Lambert-Mauriat, C.; Jacolin, C.; Bendahan, M.; Maaref, M.; Aguir, K. *Sens. Actuators, B* **2006**, *119*, 374.
- (17) Lee, D. S.; Nam, K. H.; Lee, D. D. *Thin Solid Films* **2000**, *375*, 142.
- (18) Li, Y. B.; Bando, Y.; Golberg, D.; Kurashima, K. *Chem. Phys. Lett.* **2003**, *367*, 214.
- (19) Li, Y.; Li, X.; Deng, Z.; Zhou, B.; Fan, S.; Wang, J.; Sun, X. *Angew. Chem., Int. Ed.* **2002**, *41*, 333.
- (20) Baeck, S. H.; Choi, K. S.; Jaramillo, T. F.; Strucky, G. D.; Mcfarland, E. W. *Adv. Mater.* **2003**, *15*, 1269.
- (21) Wang, S.; Feng, X.; Yao, J.; Jiang, L. *Angew. Chem., Int. Ed.* **2006**, *45*, 1264.
- (22) Li, X. L.; Lou, T. J.; Sun, X. M.; Li, Y. D. *Inorg. Chem.* **2004**, *43*, 5442.
- (23) Zhou, J.; Ding, Y.; Deng, S. Z.; Gong, L.; Xu, N. S.; Wang, Z. L. *Adv. Mater.* **2005**, *17*, 2107.

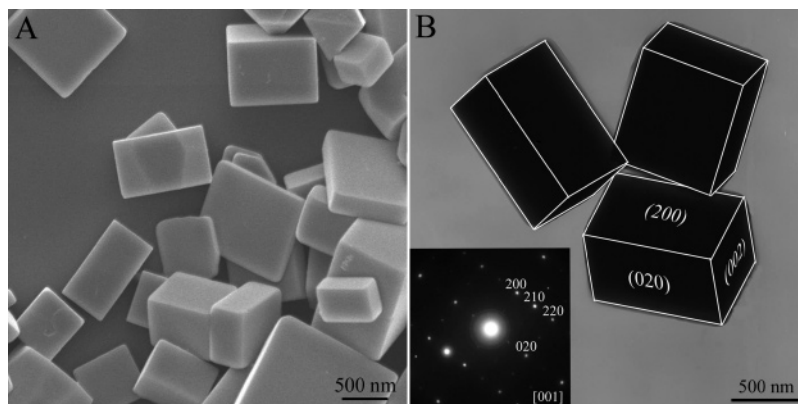


Figure 1. SEM and TEM images of $[\text{WO}_3(\text{bpy})_{0.5}]_n$ synthesized at 180 °C for 72 h with a molar ratio of WO_3 to 4,4'-bipyridine of 1:1.

thermal decomposition of the as-synthesized rectangular $[\text{WO}_3(\text{bpy})_{0.5}]_n$ ($\text{bpy} = 4,4'$ -bipyridine) precursor. The reason for the use of LMO–4,4'-bipyridine hybrid materials as the precursor for synthesizing inorganic materials in this work is the special coordination effect of the rodlike bidentate ligand 4,4'-bipyridine.

Experimental Section

Two-Step Synthesis of Rectangular $(\text{WO}_3)_n$. The method of preparation for $[\text{WO}_3(\text{bpy})_{0.5}]_n$ adopted in this work is similar to a previously reported procedure.⁹ Briefly, a solid–liquid mixture of $(\text{WO}_3)_n$ (0.116 g, >99.5%), 4,4'-bipyridine (0.096 g, $\text{C}_{10}\text{H}_8\text{N}_2 \cdot 2\text{H}_2\text{O}$, >99%), and deionized water (40 g) was transferred to a Teflon-lined stainless-steel autoclave. In this case, the molar ratio of $(\text{WO}_3)_n$ to 4,4'-bipyridine is 1:1. The hydrothermal reactions were conducted at 180 °C for 72 h. The light-yellow precipitates were collected, washed with distilled water several times, and then dried at 60 °C for 10 h. The yield of $[\text{WO}_3(\text{bpy})_{0.5}]_n$ is estimated to be higher than 95% based on the scanning electron microscopy (SEM) and X-ray diffraction (XRD) results.

The as-synthesized $[\text{WO}_3(\text{bpy})_{0.5}]_n$ crystals were then used as the precursor for the preparation of the final rectangular $(\text{WO}_3)_n$ structures. The reactions were carried out in a tubular quartz furnace at 600 °C for 30 min in air under normal atmospheric pressure.

Characterization. The crystal structures of the resulting products were characterized by XRD (Rigaku D-max- γ A XRD with Cu KR radiation, $\lambda = 1.54178$ Å). The morphologies and sizes of the resulting products were determined by field-emission scanning electron microscopy (FE-SEM, JSM 6700F) combined with energy dispersive analyses of X-ray emission (EDX), and transmission electron microscopy (TEM, JEM-2000EX) combined with selected area electron diffraction (ED), respectively. Thermal stability of the as-prepared $[\text{WO}_3(\text{bpy})_{0.5}]_n$ was investigated with thermogravimetric and differential thermogravimetric analysis (TG/DTG, Netzsch 449c) at a heating rate of 10 °C min^{-1} in air atmosphere. The samples were prepared by placing a drop of the sample suspended in anhydrous ethanol on a silicon wafer, sputtering them with thin layers of Au for SEM imaging, placing them on perforated carbon-coated copper grids, and then drying them at room temperature for TEM imaging. The acceleration voltages for SEM, TEM, ED, and EDX were 5, 160, 160, and 15 kV, respectively.

Results and Discussion

Figure 1A and its low-magnification SEM image (see Supporting Information Figure S1) reveal that the resulting products are entirely composed of rectangular-like structures

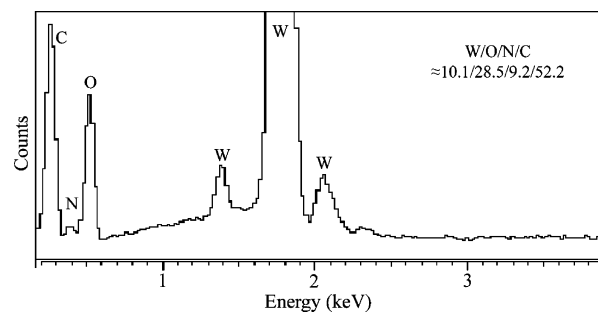


Figure 2. EDX pattern of $[\text{WO}_3(\text{bpy})_{0.5}]_n$.

with sharp corners and smooth surfaces. The edge lengths range from 400 nm to 1.5 μm . The rectangular structures of as-synthesized products are further confirmed by the TEM image (Figure 1B). The edge lengths are consistent with those in the SEM image. The ED pattern (Figure 1B inset) taken from a flat rectangular structure can be assigned to orthorhombic $[\text{WO}_3(\text{bpy})_{0.5}]_n$, which can be identified as the [001] zone axis projection of the $[\text{WO}_3(\text{bpy})_{0.5}]_n$ reciprocal lattice. And the yellowish single crystals of $[\text{WO}_3(\text{bpy})_{0.5}]_n$ are well faceted with low Miller index crystal planes of $\{200\}$, $\{020\}$, and $\{002\}$.

The formation of regular rectangular structures takes place through in situ intercalation, coordination, and self-assembly processes. Compared with the products obtained at 180 °C for 12/24 h (Figure S2A,B, Supporting Information), the morphologies become more and more regular as the reaction time is extended, which further demonstrates that the self-assembly behavior plays a significant role in the formation of regular rectangular structures. Hydrothermal treatment has many advantages in the synthesis of highly crystallized single-crystal materials. When raw $(\text{WO}_3)_n$ was hydrothermally treated at 180 °C for 72 h without 4,4'-bipyridine, only microparticles were obtained (Figure S3, Supporting Information). Therefore, over long period of time, $[\text{WO}_3(\text{bpy})_{0.5}]_n$ is easily crystallized and forms regular rectangular structures by a hydrothermal treatment process extended compared with that of $(\text{WO}_3)_n$, due to the effect of the bidentate ligand 4,4'-bipyridine. In addition, the molar ratio of 4,4'-bipyridine to $(\text{WO}_3)_n$ and reaction temperature were studied by carrying out a series of experiments with different reaction parameters. The higher molar ratio of 4,4'-bipyridine to $(\text{WO}_3)_n$ is useful in enhancing the purity and yield of rectangular $[\text{WO}_3(\text{bpy})_{0.5}]_n$

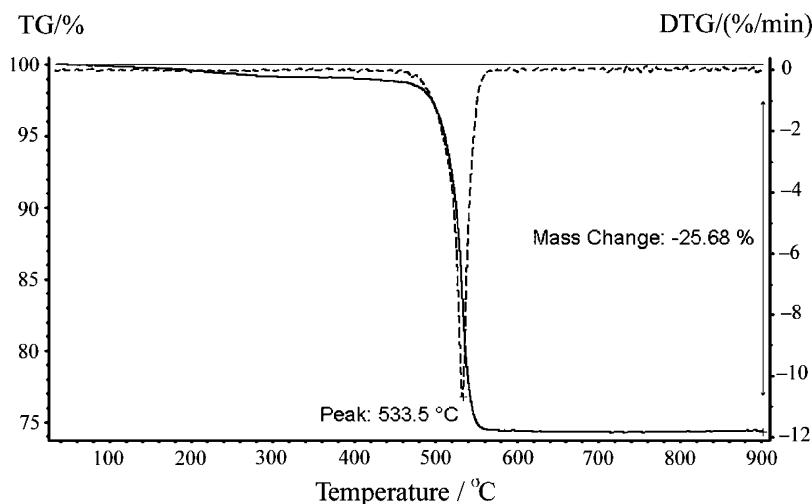


Figure 3. TG-DTG patterns of $[\text{WO}_3(\text{bpy})_{0.5}]_n$ under flowing air.

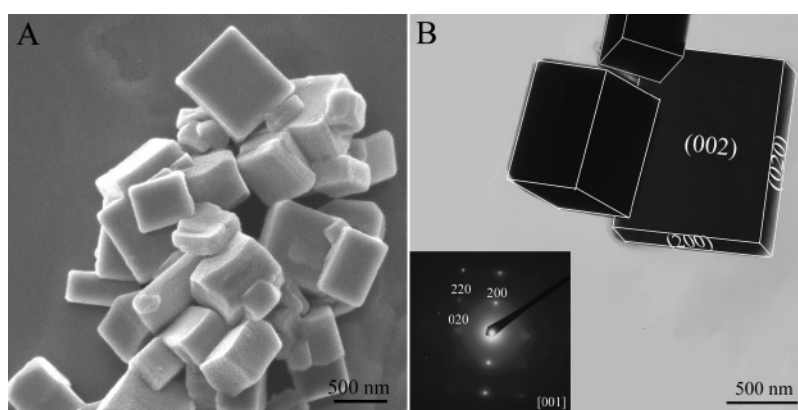


Figure 4. SEM and TEM images of rectangular $(\text{WO}_3)_n$.

(Figure S4, Supporting Information). Temperature is not an important factor in the formation of the rectangular structures, which were obtained at lower temperatures of 100–160 °C for 72 h. The elevated temperature only makes the regular structure uniform and decreases flaws (Figure S5, Supporting Information).

As expected, the atomic ratio between W and N (0.98 from the EDX result as shown in Figure 2) in the synthesized $[\text{WO}_3(\text{bpy})_{0.5}]_n$ rectangular structures is close to the theoretical value of 1, confirming the stoichiometric ratio of W to 4,4'-pyridine in this compound. The direct coordination of nitrogen to the metal cations replaces one of the oxygen atoms in $[\text{WO}_3(\text{bpy})_{0.5}]_n$.⁹ But the atomic ratio of O to W (2.82 from the EDX result is close to 3) in $[\text{WO}_3(\text{bpy})_{0.5}]_n$ does not change because the oxygen changed from being attached to only one of the W cations in $[\text{WO}_3(\text{bpy})_{0.5}]_n$ to being attached to two W cations in $(\text{WO}_3)_n$.

Furthermore, the thermal stability of $[\text{WO}_3(\text{bpy})_{0.5}]_n$ has been further tested with the TG-DTG method in Figure 3. The DTG curve (broken line) shows one endothermic peak with a maximum located at 533.5 °C. It is found that $[\text{WO}_3(\text{bpy})_{0.5}]_n$ does not show any weight loss until a temperature of 480–555 °C is obtained in an air atmosphere. The TG curve (real line) shows that $[\text{WO}_3(\text{bpy})_{0.5}]_n$ starts to decompose (weight loss) at about 480 °C. The total weight loss between 480 and 555 °C is measured to be about

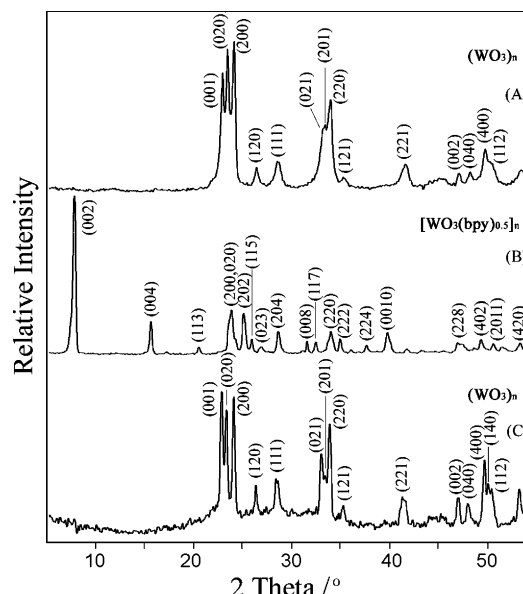


Figure 5. XRD patterns of raw $(\text{WO}_3)_n$ (A), $[\text{WO}_3(\text{bpy})_{0.5}]_n$ (B), and final $(\text{WO}_3)_n$ (C).

25.68%, which is close to the result in the literature corresponding to endothermic behavior during the thermal decomposition of $[\text{WO}_3(\text{bpy})_{0.5}]_n$ to $(\text{WO}_3)_n$.⁹ On the basis of the TG-DTG data for the intercalant 4,4'-bipyridine, the chemical stoichiometry and high thermal stability of this

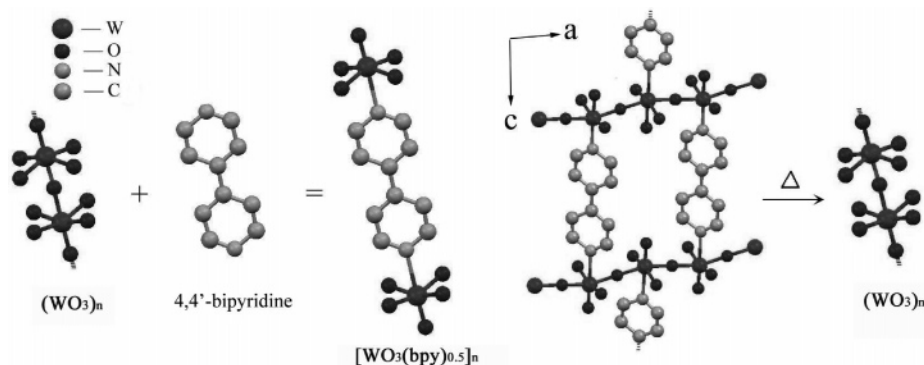


Figure 6. Schematic illustration of the evolution from $(\text{WO}_3)_n$ to $[\text{WO}_3(\text{bpy})_{0.5}]_n$ to $(\text{WO}_3)_n$.

organic–inorganic hybrid precursor are once again verified. The reason is that the W–N bond is a strong coordination bond (bond length is 2.409 Å).⁹

SEM and TEM images reveal that the rectangular shape of $(\text{WO}_3)_n$ is sustained after thermal decomposition at a heating rate of $10\text{ }^\circ\text{C min}^{-1}$ up to $600\text{ }^\circ\text{C}$ and then air cooling to room temperature (Figure 4). The edge lengths of $(\text{WO}_3)_n$ rectangular structures are in the range of 400 nm to $1\text{ }\mu\text{m}$. In comparison with $[\text{WO}_3(\text{bpy})_{0.5}]_n$ in Figure 1, the sizes of $(\text{WO}_3)_n$ rectangular structures are generally thinner than that of $[\text{WO}_3(\text{bpy})_{0.5}]_n$ for decomposition of the 4,4'-bipyridine from the interlayer space of $(\text{WO}_3)_n$. The ED pattern (Figure 4B inset) recorded on an individual $(\text{WO}_3)_n$ rectangular structure indicates that each rectangular structure is a single crystal and the final $(\text{WO}_3)_n$ structures are well faceted with low Miller index crystal planes of $\{200\}$, $\{020\}$, $\{002\}$. The (200) and (020) planes of the $(\text{WO}_3)_n$ rectangular structure become rough, and the (002) plane remains smooth compared with that of the $[\text{WO}_3(\text{bpy})_{0.5}]_n$ precursor.

XRD patterns of the raw $(\text{WO}_3)_n$ micropowder, rectangular $[\text{WO}_3(\text{bpy})_{0.5}]_n$, and final rectangular $(\text{WO}_3)_n$ are shown in parts A, B, and C of Figure 5, respectively. They show that raw $(\text{WO}_3)_n$ and the final rectangular $(\text{WO}_3)_n$ are a pure orthorhombic crystalline phase of $(\text{WO}_3)_n$ with calculated lattice constants $a = 7.38\text{ }\text{Å}$, $b = 7.51\text{ }\text{Å}$, and $c = 3.85\text{ }\text{Å}$, which is consistent with literature values (JCPDS 20-1324). $[\text{WO}_3(\text{bpy})_{0.5}]_n$ also has an orthorhombic crystalline phase (space group: $Cmca$) with calculated lattice constants $a = 7.47\text{ }\text{Å}$, $b = 7.39\text{ }\text{Å}$, and $c = 22.57\text{ }\text{Å}$.⁹ It is clear that the lattice constants of a and b are almost the same between $(\text{WO}_3)_n$ and $[\text{WO}_3(\text{bpy})_{0.5}]_n$, but the c value increases greatly, which is attributed to the intercalation of the bidentate ligand 4,4'-bipyridine. The interplanar spacing between two basal sheets ([001] direction) expands from the original $3.85\text{ }\text{Å}$ (d_{001} , $(\text{WO}_3)_n$) to $11.28\text{ }\text{Å}$ ($d_{002/2}$, $[\text{WO}_3(\text{bpy})_{0.5}]_n$). So the interlayer space for 4,4'-bipyridine intercalant can be further attained as $11.28\text{ }\text{Å} - 3.85\text{ }\text{Å} = 7.43\text{ }\text{Å}$, and the 4,4'-bipyridine was almost vertical between the $(\text{WO}_3)_n$ interlayer space for a standing 4,4'-bipyridine, which has a vertical dimension of ca. $8.8\text{ }\text{Å}$.¹⁰ Orthorhombic $(\text{WO}_3)_n$ was obtained by the thermal decomposition of $[\text{WO}_3(\text{bpy})_{0.5}]_n$. The d_{200} and d_{020} values of $(\text{WO}_3)_n$ are close to the d_{200} and d_{020} values of $[\text{WO}_3(\text{bpy})_{0.5}]_n$, which proves the lattice constants a and b change little after the decomposition of 4,4'-

bipyridine. But the interlayer spacing decreased from $11.28\text{ }\text{Å}$ ($d_{002/2}$) to $3.85\text{ }\text{Å}$ along the c axis. That is to say, there is about a two-thirds decrease along the c axis, which is in good agreement with the SEM and TEM analysis conclusion in Figures 1 and 2. The dimension decreases in large scale in the c axis direction [001], making the (200) and (020) planes become rougher than those of the rectangular $[\text{WO}_3(\text{bpy})_{0.5}]_n$ precursor.

The reaction of 4,4'-bipyridine intercalating into the interlayer space and the deposition process are illustrated in Figure 6. Orthorhombic $(\text{WO}_3)_n$ can be represented as constructed from WO_6 octahedra linked by corner sharing, an arrangement that results in a simple cubic symmetry. The bidentate ligand 4,4'-bipyridine broke one of the W–O–W bonds along the c axis and coordinated with the two W atoms by W–N coordination bonds. The direct coordination of nitrogen to the metal cations, in replacing one of the oxygen atoms, converts partially corner-sharing WO_6 octahedra into entirely corner-sharing WO_5N octahedra in $[\text{WO}_3(\text{bpy})_{0.5}]_n$. So the W–O–W structure changes to W–4,4'-bipyridine–W along with the distance increasing $7.43\text{ }\text{Å}$ (Figure 5). The structure of $[\text{WO}_3(\text{bpy})_{0.5}]_n$ consists of W/O/N layers, parallel to the ab plane, and of corner sharing $\{\text{WO}_5\text{N}\}$ octahedra bridged through 4,4'-bipyridine ligands into a 3D covalent/coordination hybrid framework. The 3D architecture can be described as an interwoven net of inorganic metal oxide layers and organic tethers. The tungsten oxide layers are stacked along the c axis in an ABAB... sequence.⁹ The formation process of the final rectangular $(\text{WO}_3)_n$ is a reverse process of the intercalation and coordination of $(\text{WO}_3)_n$ with bidentate ligand 4,4'-bipyridine, and the W–4,4'-bipyridine–W bond changed to the W–O–W bond, with the interlayer spacing decreased from 11.28 to $3.85\text{ }\text{Å}$ along the c axis.

Conclusions

In summary, we have demonstrated a LMO–organic hybrid precursor route to the preparation of rectangular $(\text{WO}_3)_n$. First, rectangular $[\text{WO}_3(\text{bpy})_{0.5}]_n$ precursor with novel crystallographic framework topologies was formed with the reaction of $(\text{WO}_3)_n$ and 4,4'-bipyridine by a process of intercalation, coordination, and self-assembly. Then rectangular $(\text{WO}_3)_n$ was fabricated by a thermal decomposi-

tion process of rectangular $[\text{WO}_3(\text{bpy})_{0.5}]_n$. The interlayer spacing changed from 3.85 to 11.28 to 3.85 Å as the 4,4'-bipyridine intercalated and decomposed in/from the interlayer space. The LMO–organic hybrid precursor route is very effective in the formation of traditional inorganic materials with novel shapes, which are hard to prepare by one-step reaction because of their crystal structure properties.

Supporting Information Available: Low-magnification SEM image of $[\text{WO}_3(\text{bpy})_{0.5}]_n$ and SEM images of $[\text{WO}_3(\text{bpy})_{0.5}]_n$ obtained with different synthesis parameters, such as different reaction times, different molar ratios of 4,4'-bipyridine to $(\text{WO}_3)_n$, and different reaction temperatures. This material is available free of charge via the Internet at <http://pubs.acs.org>.

IC701481Z